RESEARCH ARTICLE | JULY 23 2025

Chaotic transport in the drift motion for a magnetized plasma with nonlinear mode coupling

P. Haerter ; I. L. Caldas ; R. L. Viana

Phys. Plasmas 32, 072307 (2025)
https://doi.org/10.1063/5.0276163

Chaotic transport in the drift motion for a magnetized plasma with nonlinear mode coupling

Cite as: Phys. Plasmas **32**, 072307 (2025); doi: 10.1063/5.0276163
Submitted: 16 April 2025 · Accepted: 10 July 2025 ·
Published Online: 23 July 2025

P. Haerter,[1,a)] I. L. Caldas,[2] and R. L. Viana[1,3]

AFFILIATIONS

[1]Departamento de Física, Universidade Federal do Paraná, Curitiba, 81531-990 Paraná, Brazil
[2]Instituto de Física, Universidade de São Paulo, São Paulo, São Paulo, Brazil
[3]Centro Interdisciplinar de Ciência, Tecnologia e Inovação, Núcleo de Modelagem e Computação Científica, Universidade Federal do Paraná, Curitiba, 81531-990 Paraná, Brazil

[a)]Author to whom correspondence should be addressed: haerter@ufpr.br

ABSTRACT

The interplay between drift-wave coherence and particle transport in plasmas is investigated through a truncated Hasegawa–Mima model coupled with a drift-wave Hamiltonian model. By reducing the system to a three-wave interaction, we identify regimes of periodic and chaotic wave amplitudes and link them to the emergence or suppression of zonal flows. Numerical simulations reveal two distinct transport regimes: hyperballistic motion under periodic waves, where coherent zonal flows channel particles poloidally, and superdiffusive spreading under chaotic waves, where non-periodic fields disrupt directional coherence. Particle tracking indicates that periodic waves enhance radial confinement while enabling rapid poloidal transport, whereas chaotic fluctuations suppress large-scale migration through chaotic scattering. These results highlight the critical role of wave-field coherence in determining transport efficiency and offer a conceptual framework for turbulence control, highlighting that manipulating the coherence of the turbulent field, in addition to its amplitude, is a key strategy for controlling plasma transport. The findings connect reduced-order models with fully turbulent systems, offering insights into harnessing self-organized structures, such as zonal flows, for improved plasma confinement.

I. INTRODUCTION

Nuclear fusion, as a sustainable energy source, relies on the effective confinement of high-temperature plasmas within devices like tokamaks. A critical challenge in achieving this goal lies in understanding and controlling plasma turbulence, which drives anomalous transport of particles and energy across magnetic field lines, degrading confinement.[1] Among the various instabilities in tokamaks, electrostatic drift-wave turbulence in the plasma edge exercises an influence in regulating cross field transport, particularly in the low-confinement (L-mode) regime.[2] These low-frequency fluctuations, driven by density and temperature gradients, generate stochastic electric fields that induce $\mathbf{E} \times \mathbf{B}$ drifts, often resulting in chaotic particle motion.[3] The Hasegawa–Mima equation has long served as a fundamental model for studying such drift-wave dynamics,[4] capturing the nonlinear interplay between wave propagation and plasma inhomogeneity.

While some studies primarily focused on fully developed turbulence, recent advances have highlighted the critical role of coherent structures—such as zonal flows and streamers—that emerge from turbulence and strongly modulate transport.[2,5] These self-organized structures can either suppress or enhance particle diffusion, depending on their spatial and temporal coherence,[6] emphasizing the role of nonlinear wave interactions in plasma confinement.[7]

In this work, we investigate how the periodicity of drift-wave amplitudes influences particle transport in a model of magnetized confined plasma, by truncating the Hasegawa–Mima equation to a three-wave system with dissipative coupling[8] and using it as the amplitude input in the Horton drift-wave model with in the original paper disregards the mode coupling, with we try to fill this gap in the present work.[9] We select the dynamical regimes of periodic and chaotic wave amplitudes and link them to the emergence or suppression of zonal flows. Our analysis reveals two distinct transport regimes:

hyperballistic motion under periodic wave amplitudes, where coherent zonal flows channel particles poloidally, and superdiffusive transport under chaotic waves, where non periodic waves disrupt directional coherence. Using parameters from the TCABR Tokamak,[10] we numerically solve the coupled wave equations and track passive particles, such as charged impurities, advected by the resulting $\mathbf{E}\times\mathbf{B}$ flows. These findings emphasize the critical role of wave-field coherence in determining transport efficiency.

The paper is structured as follows: Section II outlines the theoretical model and numerical framework, Section III details the parameter choices and wave coupling mechanisms, Section IV presents the transport analysis across periodic and chaotic regimes, and Section V summarizes the conclusions.

II. THEORETICAL MODEL

We are primarily interested in the peripheral region of a toroidal plasma column. To facilitate analysis, we consider a slab using rectangular coordinates (x, y, z), where x represents the radial distance from the cylinder axis, $y = a\theta$ is the rectified poloidal coordinate, and $z = R\varphi$ is the rectified toroidal coordinate. The respective intervals for these coordinates are $0 \le x \le a$, $0 \le y < 2\pi a$, and $0 \le z < 2\pi R$.

In our simplified model, the toroidal field $B_\varphi \equiv B$ is assumed to be uniform and directed along the z-coordinate, while the poloidal field, is given by $B_\theta \sim \varepsilon B_\varphi$, which ε is the inverse aspect ratio. The cyclotron frequency $\omega_{ci} = eB/m_i$. We assume that the ion temperature T_i is much lower than the electron temperature T_e, making it sufficient to consider only electron motion in our analysis. For a plasma with electron temperature T_e, we define a characteristic length scale $\rho_s = \sqrt{T_e}/\omega_{ci}$, which represents the characteristic cross field shielding distance for charge clumps in the presence of drift-wave fluctuations.

In the present work, we consider electrostatic low-frequency drift instabilities, where the electric field is derived from a scalar potential as $\mathbf{E} = -\nabla\phi$. We normalize the physical quantities in the following way

$$x' = x\rho_s, \quad y' = y\rho_s, \quad t' = \omega_{ci}t, \quad \phi' = \frac{e\phi}{T_e}. \tag{1}$$

The respective definition intervals for these coordinates are $0 \le x' \le L_x \equiv a/\rho_s$ and $0 \le y' \le L_y \equiv 2\pi a/\rho_s$.

The description of drift instabilities is two-dimensional, in a plane perpendicular to the magnetic field, such that $\mathbf{r} = (x', y')$. The gradients are thus given by $\nabla = (\partial/\partial x, \partial/\partial y)$, where we dropped the primes in the coordinates for simplicity.

Electrostatic fluctuations in the plasma edge are driven by a plasma density gradient.[2] The electrostatic potential $\phi(\mathbf{r}, t)$ is a solution to the Hasegawa–Mima equation[4] given by

$$\frac{\partial}{\partial t}\left(\nabla^2\phi - \phi\right) - \left[(\nabla\phi\times\hat{\mathbf{z}})\cdot\nabla\right]\left[\nabla^2\phi - \ln\left(\frac{n_0}{\omega_{ci}}\right)\right], \tag{2}$$

where we have dropped the primes for notational simplicity. Under the quasi-neutrality condition, the electron and positive ion densities are equal and given by a Boltzmann distribution.

It is important to situate the Hasegawa–Mima equation within the landscape of modern plasma theory. The equation is a reduced electrostatic fluid model based on several key assumptions, most notably the adiabatic response of electrons. As has been extensively shown in recent gyrokinetic studies, this assumption breaks down in the edge of high-performance Tokamaks, where non-adiabatic and electromagnetic effects become dominant drivers of transport.[11]

The description of electrostatic turbulence from the Hasegawa–Mima equation assumes the presence of an electrostatic drift wave at a low frequency $\omega \ll \omega_{ci}$. Such a wave exists if its phase velocity along the magnetic field satisfies $v_{Ti} < v_T < v_{Ei}$, where $v_{Ti,e}$ are the thermal velocities for ions and electrons, respectively.[3] The dispersion relation of a drift wave is given by

$$\omega = \frac{1}{1+k^2}\left[(\mathbf{k}\times\hat{\mathbf{z}})\cdot\nabla\ln\left(\frac{n_0}{\omega_{ci}}\right)\right], \tag{3}$$

where ω is the drift-wave frequency and $\mathbf{k}$ is the wave vector in the plane perpendicular to the magnetic field.

We look for solutions of the Hasegawa–Mima equation, in the case of N drift waves, in the following form (2)

$$\phi(\mathbf{r}, t) = \frac{1}{2}\sum_{j=1}^{N}\left\{\phi_{\mathbf{k}_j}(t)e^{i\mathbf{k}_j\cdot\mathbf{r}} + \phi^*_{\mathbf{k}_j}(t)e^{-i\mathbf{k}_j\cdot\mathbf{r}}\right\}, \tag{4}$$

where $\mathbf{k}_j = (k_{jx}, k_{jy})$ is the propagation vector of the jth wave along the directions transversal to the magnetic field, and $\phi_{\mathbf{k}_j}$ are the corresponding time-dependent Fourier modes.[1]

Substituting the expansion (4) into the Hasegawa–Mima equation (2) leads to an infinite system of coupled differential equations for the Fourier modes

$$\frac{d\phi_{\mathbf{k}}}{dt} + i\omega_{\mathbf{k}}\phi_{\mathbf{k}} = \sum_{\mathbf{k}_\alpha,\mathbf{k}_\beta,\mathbf{k}_\gamma}\Lambda^{\mathbf{k}_\alpha}_{\mathbf{k}_\beta,\mathbf{k}_\gamma}\phi^*_{\mathbf{k}_\beta}\phi^*_{\mathbf{k}_\gamma}, \tag{5}$$

where the summation is over wavevectors that satisfy the triplet relation

$$\mathbf{k}_\alpha + \mathbf{k}_\beta + \mathbf{k}_\gamma = 0, \tag{6}$$

for any choice of $\mathbf{k}$, with the coupling coefficients given by

$$\Lambda^{\mathbf{k}_\alpha}_{\mathbf{k}_\beta,\mathbf{k}_\gamma} = \frac{(k_\gamma^2 - k_\beta^2)}{2(1+k_\alpha^2)}(\mathbf{k}_\beta\times\mathbf{k}_\gamma)\cdot\hat{\mathbf{z}}. \tag{7}$$

From a dynamical perspective, an autonomous flow can exhibit chaotic solutions when its dimension is equal to or greater than three.[12] Based on this, and since only a few Fourier modes are required to adequately describe the development of weak turbulence,[1,8,13] we truncate the infinite set of equations to consider only three-wave interactions, with wavevectors $\mathbf{k}_1$, $\mathbf{k}_2$, and $\mathbf{k}_3$.

We introduce a dissipative term that describes the energy exchange between modes,[14] in the form $\mu_j\phi_{\mathbf{k}_j}$ for $j = 1, 2, 3$, where μ_j are the growth and decay coefficients. This represents a deliberate departure from the ideal, inviscid Hasegawa–Mima equation, which is a conservative system that conserves two quadratic invariants: energy and potential enstrophy.

The coefficients μ_j are phenomenological terms designed to model a more realistic open, driven-dissipative system. The positive growth rate models the energy input from a primary instability (the "pump" wave), while the negative decay rates model an energy sink, representing either physical dissipation or the transfer of energy to modes outside of our three-wave truncation. Consequently, the introduction of the non-zero μ_j terms explicitly breaks the conservation laws for the subsystem of the three interacting modes.

With this consideration, Eq. (5) can be simplified to the following set of $N = 3$ coupled differential equations

$$\frac{d\phi_1}{dt} + i\omega_1\phi_1 = \Lambda^1_{2,3}\phi^*_2\phi^*_3 + \mu_1\phi_1, \tag{8}$$

$$\frac{d\phi_2}{dt} + i\omega_2\phi_2 = \Lambda^2_{3,1}\phi^*_3\phi^*_1 + \mu_2\phi_2, \tag{9}$$

$$\frac{d\phi_3}{dt} + i\omega_3\phi_3 = \Lambda^3_{1,2}\phi^*_1\phi^*_2 + \mu_3\phi_3. \tag{10}$$

We represent the Fourier modes of Eq. (4) as

$$\phi_{\mathbf{k}_j}(t) = A_j(t)e^{-i(\omega_j t-\beta_j)}, \tag{11}$$

where ω_j are the associated frequencies of each drift wave, $A_j = |\phi_{\mathbf{k}_j}(t)|$ the respective amplitudes, and β_j are phase constants.[15] Substituting (11) into (4), we obtain

$$\phi(\mathbf{r}, t) = \sum_{j=1}^{3} A_j(t)\cos(\mathbf{k}_j\cdot\mathbf{r} - \omega_j t + \beta_j), \tag{12}$$

which describes the electrostatic potential that acts inside the plasma in the presence of the drift wave instabilities.

Since we are dealing with propagation in the radial and poloidal directions (represented by the x and y directions, respectively), with a constant magnetic field along the z-direction, the gyrating plasma particles undergo a $\mathbf{E}\times\mathbf{B}$ drift motion, with velocity

$$\mathbf{v}_\mathbf{E} = \frac{\mathbf{E}\times\mathbf{B}}{B^2} = -\frac{E}{B}\hat{\theta} \tag{13}$$

along the poloidal direction.

Considering a time-dependent electric potential $\phi(x, y, t)$ related to the propagating drift waves, the equations of the $\mathbf{E}\times\mathbf{B}$ drift motion can be rewritten as

$$v_x = \frac{dx}{dt} = -\frac{1}{B_0}\frac{\partial}{\partial y}\phi(x, y, t), \tag{14}$$

$$v_y = \frac{dy}{dt} = \frac{1}{B_0}\frac{\partial}{\partial x}\phi(x, y, t), \tag{15}$$

which are canonical equations for the Hamiltonian $H = \phi/B_0$, such that (x, y) are canonically conjugated momentum-coordinate variables. In the following, we consider that the particle guiding centers undergo $\mathbf{E}\times\mathbf{B}$-drift motion without influencing the fields themselves, i.e., we are treating here a passive advection under $\mathbf{E}\times\mathbf{B}$-drift flow.

In order to set up the proper boundary conditions, we impose some constraints related to the propagating drift waves in the x and y directions. For the y direction, we require an integer multiple of the wavelength to match the propagation interval $L_y = m\lambda_y$, where $m \in \mathbb{Z}^*$. The corresponding wavenumber will be

$$k_y = \frac{2\pi}{\lambda_y} = \frac{2m\pi}{L_y}. \tag{16}$$

On the other hand, for the radial direction, the drift waves are stationary, so the waves vanish at the boundaries, $x = 0$ and $x = L_x$. This implies half-integer wavenumbers in the propagation interval: $L_x = n\lambda_x/2$, where $n \in \mathbb{Z}^*$, such that

$$k_x = \frac{2\pi}{\lambda_x} = \frac{n\pi}{L_x}. \tag{17}$$

Applying these boundary conditions and the respective wavenumbers, we get[9]

$$\phi(x, y, t) = \sum_{j=1}^{3} A_j(t)\sin(k_{jx}x + \beta_j)\cos(k_{jy}y - \omega_j t). \tag{18}$$

Substituting these relations in the wavevector restriction imposed by the Hasegawa–Mima equation (6), we obtain a pair of constraints on the integer mode numbers, namely,

$$n_1 + n_2 + n_3 = 0, \quad m_1 + m_2 + m_3 = 0. \tag{19}$$

Taking these boundary conditions into account, our theoretical model for drift motion under drift waves with nonlinear mode coupling, given by (18) consists of the following equations:

$$\frac{dx}{dt} = \sum_{j=1}^{3} k_{jy}A_j(t)\sin(k_{jx}x + \beta_j)\sin(k_{jy}y - \omega_j t), \tag{20}$$

$$\frac{dy}{dt} = \sum_{j=1}^{3} k_{jx}A_j(t)\cos(k_{jx}x + \beta_j)\cos(k_{jy}y - \omega_j t), \tag{21}$$

which can be solved in parallel with the nonlinear mode coupling equations, Eqs. (8)–(10).

III. PARAMETER VALUES

The system of coupled differential equations for the particle drift coordinates and the drift wave amplitudes can be numerically solved, given initial conditions for the guiding center position $(x(0), y(0))$ as well as the mode amplitudes $\phi_i(0)$, $i = 1, 2, 3$. Parameter values were taken from the TCABR Tokamak, operating at the Institute of Physics, University of Sao Paulo, Brazil. For this device, the toroidal magnetic field is $B = 0.4$ T (at the magnetic axis), the central electron temperature is $T_e = 10$ eV, the electron density gradient is $|\nabla n_0|/n_0 = 5\,\mathrm{m}^{-1}$, and the ion-cyclotron frequency is $\omega_{ci} = 1.05\times10^8$ Hz. The corresponding length scale is $\rho \approx 10^{-3}$ m.[10,16]

Based on particle flux measurements, the radial density gradient $\mathcal{N}$ at the plasma edge was estimated[16] as

$$\mathcal{N} := \rho_s\left|\nabla\ln\left(\frac{n_0}{\omega_{ci}}\right)\right| = \rho_s\left|\frac{\nabla n_0}{n_0}\right| \approx 10^{-3}. \tag{22}$$

Our interest lies in the dynamics within a small region inside the plasma. By considering that the Hasegawa–Mima equation assumes the wave primarily propagates in the x-y plane, we focus on the dynamics on this plane, with a constant z. This assumption allows us to disregard the z-components of the wave vectors, setting these to zero.

Measurements of the potential edge fluctuations using electrostatic probes indicate a poloidal wave number k_θ in the range of $(1-5)\times10^3\,\mathrm{m}^{-1}$, with a broad spectral content and a pronounced feature at $\omega_{\exp} \approx 50$ kHz.[16,17] Based on the experimental value of the dominant poloidal wave number of plasma edge fluctuations, we choose $k_\theta = k_{1y} = 3\times10^3\,\mathrm{m}^{-1}$. From this value, it follows that the corresponding normalized value of $k_{1y} = 3$, which implies that $m_1 = 6$ for $L_y = 4\pi$. In order to get nondimensional wave frequencies,

we used the ratio of the plasma frequency $\omega_{\exp}$ to the ion-cyclotron frequency, scaled by the order of the wavenumbers, and obtained $\omega_1 = \omega_2 = \omega_3 = 0.476$.

From Eq. 3 we obtain the dispersion relation for drift waves,

$$\omega_j = -\frac{(k_{jy} - k_{jx})}{1 + k_j^2}\mathcal{N}, \tag{23}$$

which allows us to evaluate the coupling coefficient, from Eq. (7), as

$$\begin{aligned}\Lambda_1 = \mathbf{\Lambda}^1_{2,3} &= \frac{(k_3^2 - k_2^2)}{2(1 + k_1^2)}(\mathbf{k}_2 \times \mathbf{k}_3)\cdot\hat{\mathbf{z}} \\ &= \frac{\omega_1}{2\mathcal{N}}\frac{k_3^2 - k_2^2}{k_{1y} - k_{1x}}(k_{2x}k_{3y} - k_{2y}k_{3x}).\end{aligned} \tag{24}$$

For the remaining values of the wavevector components, we choose a set of values that produce a stable solution within the constraints of the model. In Table I, we summarize the n and m values for the chosen wave vectors, as well as the normalized wave frequencies used and the coupling constants.

The energy exchange coefficients μ_j can be estimated by assuming that the pump mode ϕ_3 induces the process of energy redistribution among the daughter modes ϕ_1 and ϕ_2. To achieve this, the pump mode has a positive exchange coefficient μ_1, which increases its value over time until it transfers energy to the other modes that have negative exchange rates ($\mu_{2,3}$). Their numerical values are adjusted to obtain stable solutions for the system and to provide wave-mode amplitudes in the range observed in the experiments of plasma edge fluctuations between ± 20 V. We set $\mu_3 = 0.07$ and $\mu_1 = \mu_2 < 0$, with μ_1 being the control parameter for the numerical simulations and the only free parameter in the system, are just control parameters and do not correspond to a real parameter that can be controlled.

For the numerical simulations presented in this work, the initial conditions of the wave amplitudes are chosen as

$$\begin{aligned}&\mathrm{Re}\,\phi_1(0) = \mathrm{Re}\,\phi_2(0) = \mathrm{Re}\,\phi_3(0) = 0.01,\\ &\mathrm{Im}\,\phi_1(0) = \mathrm{Im}\,\phi_2(0) = \mathrm{Im}\,\phi_3(0) = 0.00,\end{aligned}$$

such that the nonlinear mode equations, Eqs. (8)–(10), were numerically integrated using the Adams–Bashforth–Moulton method from the Boost package.[18]

It is known that the system of coupled wave equations exhibits both chaotic and periodic behavior for appropriate values of $\mu_1 = \mu_2$, using the set of values from Table I for the remaining parameters.[8] The dependence of the dynamics on the control parameter is shown in the bifurcation diagram depicted in Fig. 1(a), constructed from the local maxima of $|\phi_3|$, which is similar to a stroboscopic map derived from the time series and reveals changes in the wave period. Figure 1(b) shows a typical periodic trajectory with period 1, where it is possible to see the pump mode $|\phi_3|$ transferring its energy to the auxiliary (daughter) modes $|\phi_1|$ and $|\phi_2|$. Figures 1(c) and 1(d) represent two other types of time series: one with period 2 and one exhibiting chaotic behavior.

TABLE I. Set of numerical values used for all the simulations, where j is the wave index.

j	n_j	m_j	ω_j	Λ_j
1	12	6	0.476	71.400
2	−7	−3	0.476	651.50
3	−5	−2	0.476	−1088.8

To explore how different values of μ_1 affect the transport in the system, we selected several values across different regions of the bifurcation diagram shown in Fig. 1. We chose eight distinct values of μ_1 that produce periodic wave amplitudes, ranging from waves with a period of 1–5. Additionally, we selected four values of μ_1 from the chaotic regions, which lie between the periodic regimes. By varying the control parameter across both periodic and chaotic regions (see Table II), we identified distinct transport behaviors linked to wave coherence and zonal flow formation.

IV. CHAOTIC TRANSPORT

In order to analyze the transport dynamics induced by drift waves, we choose an ensemble of passive particles initially distributed within a confined spatial region. Their dynamics were then evolved using Eqs. (20) and (21), with the wave amplitudes generated by Eqs. (8)–(10). By tracking their trajectories over time, we extracted critical transport properties of the system. The particles were initialized in the domain $x \in (-\pi, \pi)$ and $y \in (-2\pi, 2\pi)$, and evolved until a final time of $T_f = 10^4$ using a fourth-order Runge–Kutta integrator with a time step of $dt = 10^{-3}$.

By using a Poincaré map, we can observe the patterns of particle motion by considering the periodicity of the stroboscopic mapping, obtained by sampling the values of x and y for each particle at times $t_n = nT$, where we used the period of the parent wave $T = 2\pi/\omega_1$. Figure 2 illustrates this map for different values of μ_1. A clear distinction emerges between the two groups of cases. For chaotic amplitudes, as shown in Figs. 2(a) and 2(c), the phase space exhibits significant disorder, with particles spreading diffusely throughout the region without any apparent organization. On the other hand, for periodic waves [Figs. 2(b) and 2(d)], coherent structures appear, chiefly along $x = const.$ lines. These structures reveal a well-defined division between transport regions, indicating the presence of transport barriers that confine particle movement to specific x regions. The absence of Kolmogorov–Arnold–Moser (KAM) islands in Fig. 2 is a direct consequence of the system's strongly non-autonomous nature. The Hamiltonian that governs the particle motion is explicitly time-dependent due to the evolving wave amplitudes and phases.

According to the Kolmogorov–Arnold–Moser (KAM) theorem, the persistence of invariant tori (which appear as regular KAM curves in a Poincaré map) is only guaranteed for sufficiently small perturbations of an integrable system, and sufficient irrationality of the tori winding number. In our model, the wave amplitudes are chosen to be physically significant, which places the system in a strong perturbation regime where the conditions of the KAM theorem are no longer met. This strong, time-dependent forcing is sufficient to destroy the majority of the invariant tori, leading to the observed state of global chaos instead of regular orbits, even in the cases where the driving waves are perfectly periodic.

We use some diagnostic measures that capture various characteristics of the dynamics to quantify how distinct drift waves influence particle transport in plasmas. In particular, we consider the mean square displacement (MSD), which provides a global characterization of chaotic transport, and the total displacement, which is able to reveal

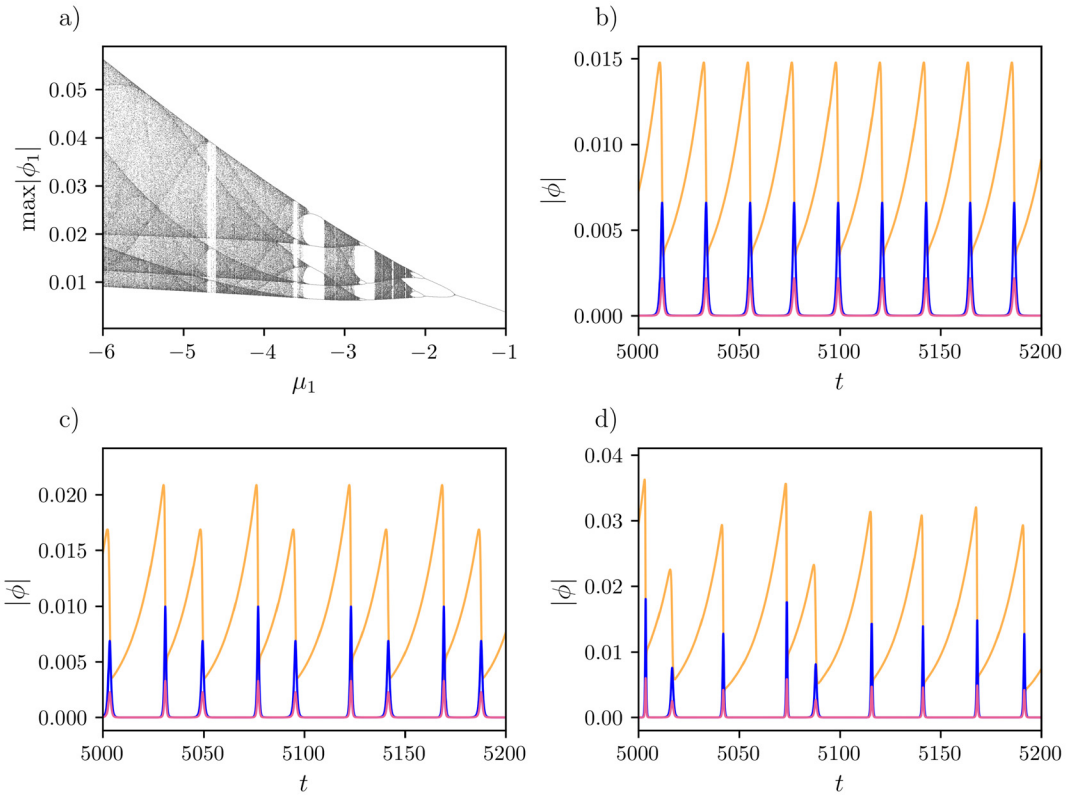

FIG. 1. (a) Bifurcation diagram for the Poincaré section $\max|\phi_3(t)|$ for varying $\mu_1 = \mu_2$ and $\mu_3 = 0.07$, showing the periodic and chaotic windows. Time series of the wave amplitude $|\phi_j|$ ($j = 1$: pink line, $j = 2$: blue line, $j = 3$: gold line) for $\mu_3 = 0.07$. (b) Time series for $\mu_1 = \mu_2 = -1.5$, showing a wave with period 1. (c) Time series for $\mu_1 = \mu_2 = -1.9$, showing a wave with period 2. (d) Time series for $\mu_1 = \mu_2 = -3.0$, showing a chaotic wave.

TABLE II. Values of the parameter μ_1 and the period of the correspondent orbit.

μ_1	Period	μ_1	Period
−1.50	1	−3.00	Chaos
−1.90	2	−3.30	5
−2.07	4	−3.60	5
−2.40	4	−4.00	Chaos
−2.50	Chaos	−4.60	3
−2.67	3	−6.00	Chaos

the inhomogeneous character of transport, since there are plasma regions for which the transport fluxes are more intense than others.

A. Mean square displacement

For a statistical characterization of transport, we computed the mean square displacement (MSD)

$$\langle \sigma(t)^2 \rangle = \frac{1}{N}\sum_{i=1}^{N} |\mathbf{x}_i(t) - \mathbf{x}_i(0)|^2, \tag{25}$$

where N denotes the total particle number and $\mathbf{x}$ denotes the position vector. The exponent of the temporal scaling $\langle \sigma(t)^2 \rangle \propto t^{\alpha}$ classifies the diffusion regime: subdiffusive ($\alpha < 1$), normal ($\alpha = 1$), superdiffusive ($1 < \alpha < 2$), ballistic ($\alpha = 2$), and hyperballistic ($\alpha > 2$).

Our analysis reveals two distinct regimes of anomalous transport, characterized by different scaling exponents (α), which emerge as a direct consequence of the wave amplitude's behavior. Periodic and chaotic waves induce fundamentally different dynamics in the system, leading to a transition in the MSD scaling from hyperballistic values ($\alpha \approx 2.1$) to superdiffusive values ($\alpha \approx 1.4$). Specifically, waves with periodic behavior drive the hyperballistic regime, significantly enhancing the transport of passive particles. In contrast, particles exhibit reduced transport when the wave amplitude is governed by chaotic dynamics, as reflected in the lower scaling exponent. These results highlight the critical role of wave amplitude modulation in governing particle transport within the plasma.

Notably, the chaotic nature of the waves suppresses diffusion compared to the periodic case, suggesting that periodic structures in the wave field allow a more efficient particle transport. Figure 3 summarizes the MSD scaling across the parameter space detailed in Table II, revealing a clear distinction between two groups: one corresponding to chaotic waves (lower α values) and the other to periodic waves (higher α values).

The observed diffusion exponent provides a quantitative measure of the transport regimes and their underlying mechanisms. The

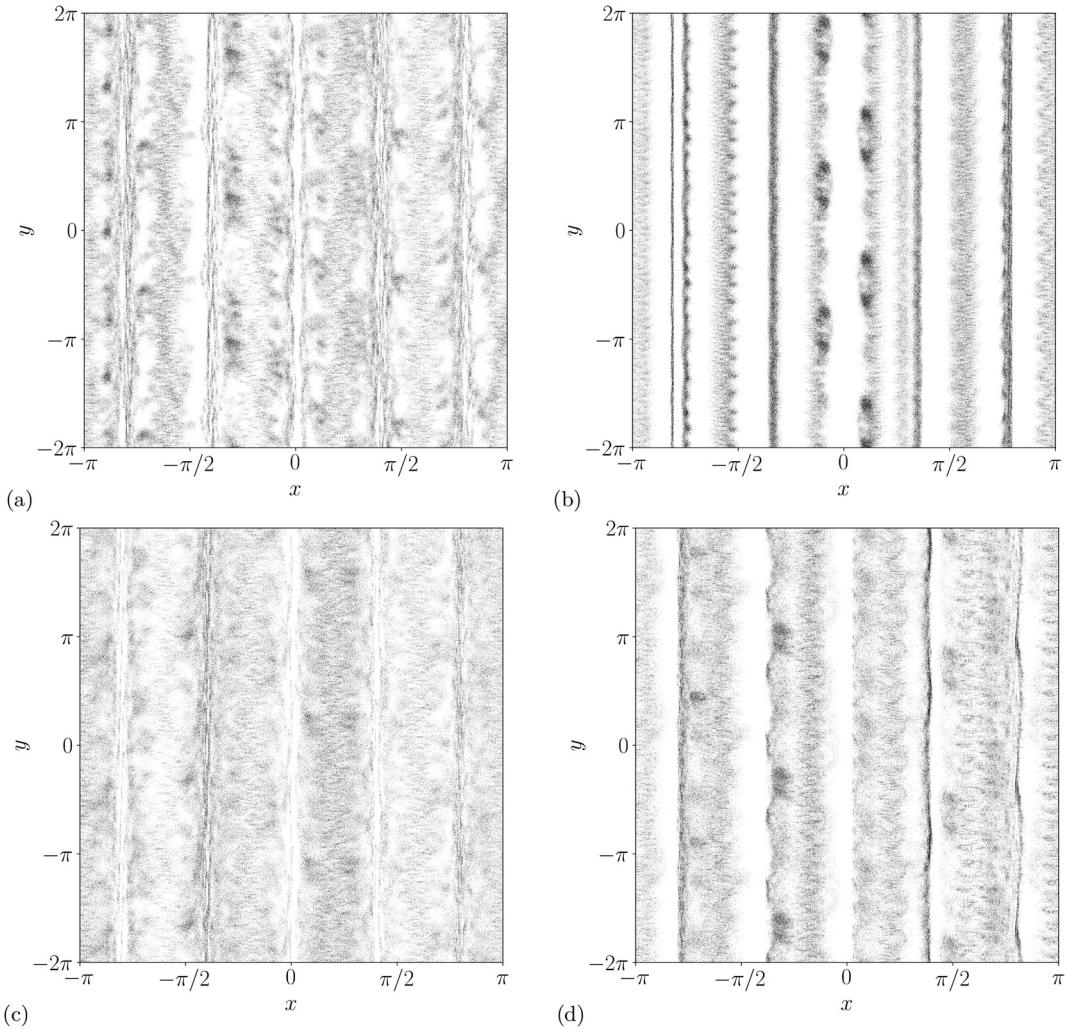

FIG. 2. Phase portrait for the Poincaré map for different values of the control parameter μ_1. Panels (a) and (c) correspond to chaotic wave amplitudes, while panels (b) and (d) correspond to periodic wave amplitudes. The specific value of μ_1 and its period are: (a) −3.0 (Chaotic) (b) −3.3 (Period 5) (c) −4.0 (Chaos) and (d) −4.6 (Period 3).For periodic waves, coherent transport barriers and zonal flow structures are evident along lines of constant *x*, whereas chaotic waves lead to diffuse, space-filling particle spreading.

hyperballistic regime observed for periodic waves suggests a highly correlated, non-diffusive process, where particles experience sustained acceleration or directional coherence. This behavior is reminiscent of coherent structures in plasma turbulence, such as zonal flows or streamers, which efficiently channel particles. This phenomenon arises from particles "surfing" the washboard potential generated by periodic waves—a spatially ordered structure that imposes coherent gradients, enabling particles to phase-lock and gain velocity linearly over time.[19,20] Such dynamics mirror the role of coherent structures like zonal flows or streamers in plasma turbulence, which channel particles efficiently by suppressing non-periodic diffusion.[21]

Our results can be compared with prior studies of transport in flows governed by the full Hasegawa–Mima equation. Other investigations have also found that superdiffusive transport can arise from electrostatic turbulence, a phenomenon attributed to the presence of "chaotic jets."[22]

The complex, time-dependent flow in our chaotic regime is analogous to the turbulent flow with embedded chaotic jets. In contrast, the highly organized zonal flows that appear in our periodic regime, which lead to hyperballistic transport, can be seen as an extreme, coherent form of such a jet. This comparison is particularly clear in what has been described as the 'anisotropic field case', where the flow becomes quasi-one-dimensional. This is directly comparable to our periodic regime, where strong zonal flows create a highly anisotropic transport environment, with particle motion overwhelmingly channeled in the y direction, as shown in our Fig. 5.

In contrast, the superdiffusive regime under chaotic waves indicates a loss of coherence. Here, the washboard potential is replaced by a non-periodic field, where particles experience intermittent kicks

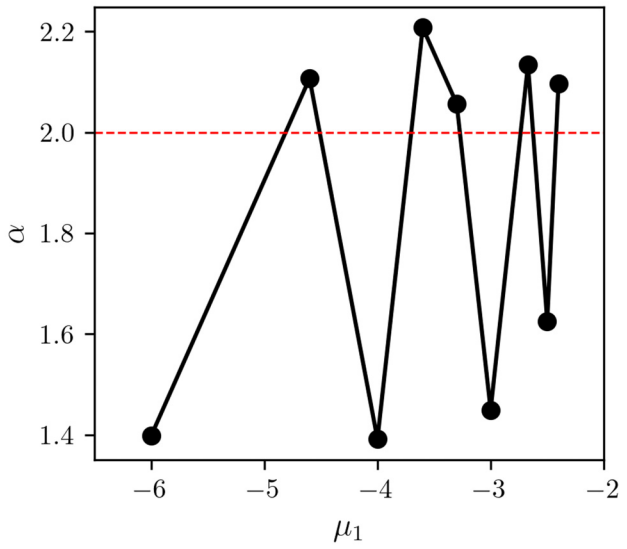

FIG. 3. The scaling exponent α as a function of the μ_1 parameter. For periodic wave amplitudes, the particles exhibit hyperballistic motion ($\alpha > 2$), while for chaotic wave amplitudes, the particles exhibit superdiffusive motion ($1 < \alpha < 2$).

from transient structures rather than sustained forcing. The reduction in α for chaotic waves highlights the role of stochasticity in suppressing large-scale transport, as particles become trapped in transient structures or experience frequent scattering, disrupting ballistic motion.

A notable feature of our results is the complete absence of a normal diffusive regime ($\alpha = 1$), which is a direct consequence of the particle transport model employed.

In the periodic regime, particles are channeled by coherent zonal flow structures, leading to long, uninterrupted flights that produce hyperballistic transport. In the chaotic regime, the driving field, while aperiodic, is not random noise but actually a deterministic chaotic field with significant spatiotemporal correlations. This leads to a correlated random walk that manifests as superdiffusion.

A normal diffusive regime would likely emerge with the inclusion of an additional stochastic process, such as collisions or background noise in the particle equations of motion, which would serve to decorrelate the particle trajectories over time. As our focus is on the transport driven purely by the specified drift-wave field, such a term was not included, and the resulting transport is consequently anomalous across all parameter regimes studied.

B. Total particle displacement

The total displacement of particles (Δ) is defined as the Euclidean distance between their initial and final positions, providing critical insights into both the magnitude and directionality of transport. Unlike the MSD that quantifies dispersion, total displacement highlights a net migration of the particles. By analyzing Δ alongside directional displacements ($\Delta x, \Delta y$), we can observe the same two groups present in the MSD analysis: a high transport governed by the periodic waves and a more diffuse transport when the periodicity of wave amplitudes is chaotic.

The total displacement, $\Delta = \sqrt{(\Delta x)^2 + (\Delta y)^2}$, provides a global measure of particle movement, while its Cartesian components Δx and Δy reveal anisotropic transport characteristics. By comparing displacements across spatial regions after fixed integration times, we identified areas of enhanced transport and preferential particle motion directions.

For chaotic wave amplitudes, the distribution of total displacement exhibits a continuous decay with no preferred magnitude [Fig. 4(a)], reflecting isotropic dispersion and suppressed net migration. Particles in these regimes experience frequent dispersion within non-periodic fields, trapping them in transient structures. This suppression of large-scale migration aligns with the subdiffusive MSD scaling, where non-periodic fluctuations disrupt coherent motion. In contrast, periodic waves generate a bimodal displacement distribution [Fig. 4(b)], with peaks at both low and high Δ. The low Δ peak corresponds to particles transiently trapped in localized regions, while the high Δ peak reflects particles in the zonal flow regions.

Figure 5 illustrates the type of displacement observed for different wave behaviors. The first and third rows correspond to cases with chaotic wave amplitudes, while the second and fourth rows show cases with periodic wave amplitudes. The first column presents the total traveled distance, while the second and third columns display the x and y components of the displacement, respectively.

The displacement metric reinforces the separation of transport regimes observed in Fig. 2. For chaotic wave amplitudes, Figs. 5(a) and 5(g) exhibit a non-homogeneous mixture of particle trajectories with no coherent spatial organization. This isotropy reflects frequent scattering, suppressing net migration by trapping particles in transient structures. In contrast, periodic waves [Figs. 5(d) and 5(j)] generate well-defined zonal flow patterns channeling particles into coherent streams. These figures also correlate the wave amplitude with the traveling distance, showing that the total distance increases from

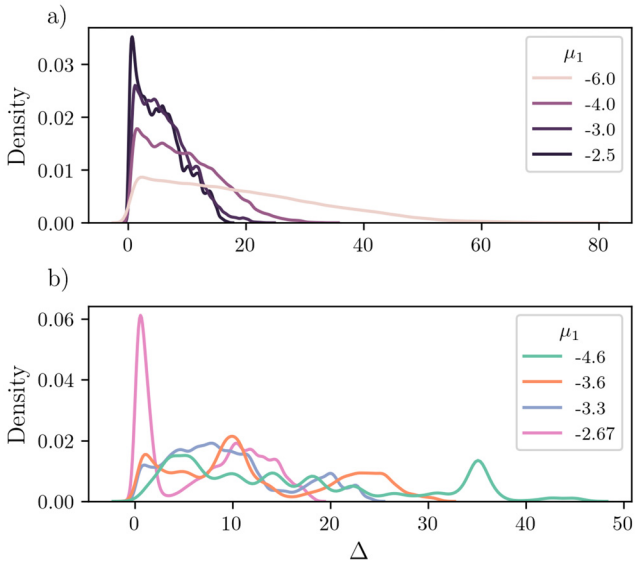

FIG. 4. Distribution of the total displacement Δ of the particles advected by two different groups of amplitude wave: (a) chaotic wave amplitudes and (b) periodic wave amplitudes.

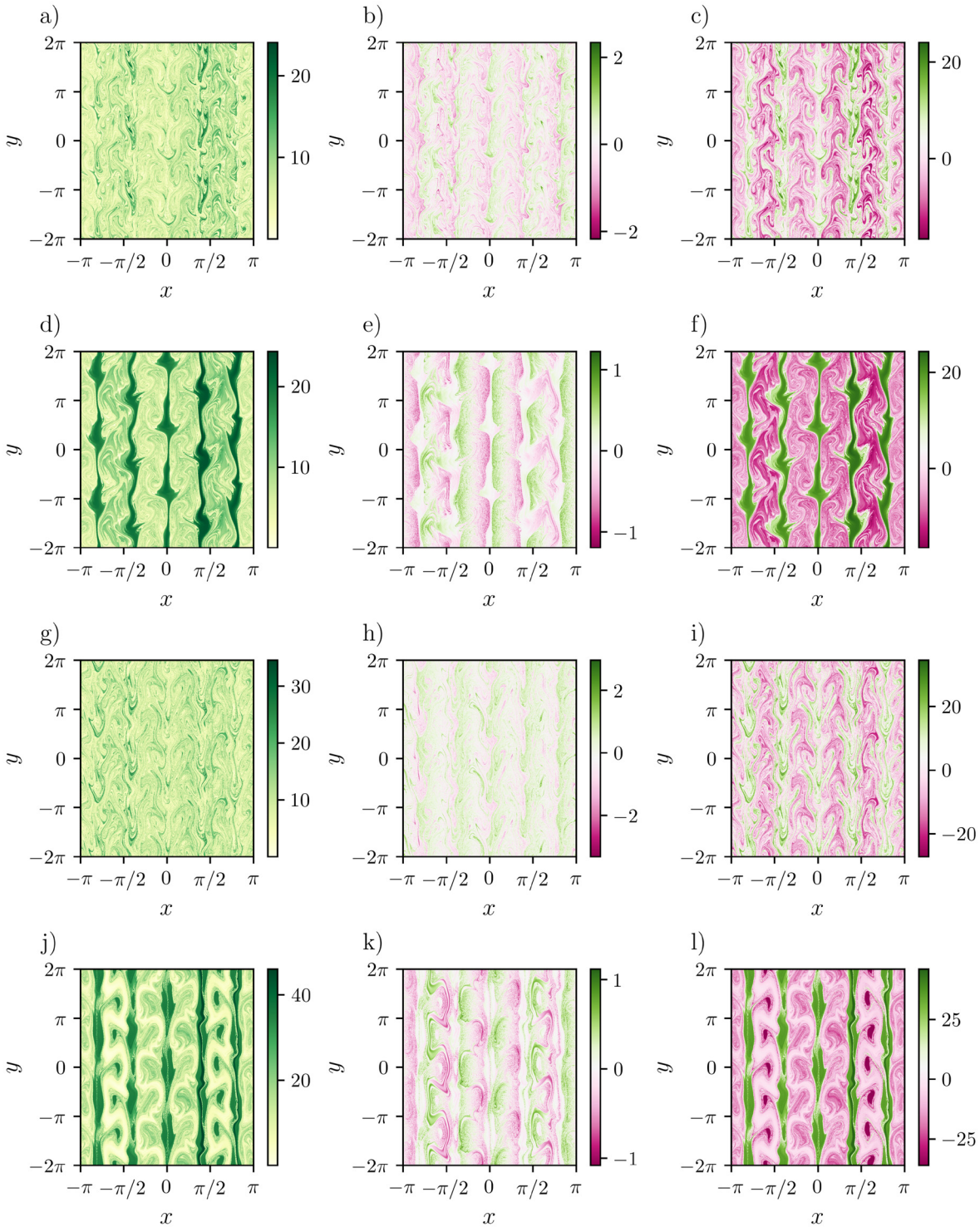

FIG. 5. Displacement of particles advected by Eqs. (20) and (21) presenting the total displacement Δ and its components in the x and y directions for the columns on the right, center, and left, respectively. The different rows correspond to different μ_1 values and periodicities: (a)–(c) $\mu_1 = -3.0$ (Chaos) (d)–(f) $\mu_1 = -3.3$ (Period 5) (g)–(i) $\mu_1 = -4.0$ (Chaos), and (j)–(l) $\mu_1 = -4.6$ (Period 3). In the chaotic regimes, a sparse distribution of displacements is observed with no regular structure formation. In contrast, the periodic regimes show the formation of well-defined zonal flows, mainly driven by displacements in the poloidal direction.

$\max|\Delta| \approx 25$ when the maximum wave amplitude is $\max|\phi_3| \approx 0.022$ to $\max|\Delta| \approx 45$ when $\max|\phi_3| \approx 0.04$.

The dominance of poloidal displacement (Δy) across all regimes, as seen in Figs. 5(c), 5(f), 5(i), and 5(l), arises from the alignment of particle motion with $\mathbf{E} \times \mathbf{B}$ flows. In magnetized plasmas, particles are constrained to follow magnetic field lines primarily along the poloidal (y) direction, while radial (x) transport requires cross field drifts or turbulence. For periodic waves, coherent $\mathbf{E}$ fields organize into zonal flows, driving particles along y with minimal radial leakage due to self-generated shear layers [Figs. 5(e) and 5(k)]. Chaotic waves disrupt this ordering, scattering particles isotropically [Figs. 5(b) and 5(h)], though residual magnetic field alignment ensures that Δy remains larger than Δx.

As the parameter μ_1 increases from the chaotic to the periodic regions in the bifurcation diagram, coherence is enhanced rather than chaos. Despite expectations of turbulent diffusion at higher μ_1, the system self-organizes into zonal flows. These flows act as transport channels, as can be seen in the high Δy regions of Figs. 5(f) and 5(l).

Zonal flows manifest as alternating bands of high and low particle density in the poloidal direction [Figs. 5(d) and 5(j)], resembling atmospheric jet streams. These flows generate shear layers at radial interfaces where velocity gradients tear apart turbulent eddies, suppressing radial transport. This dual role, enhancing poloidal migration while confining particles radially, explains the stark contrast between chaotic and periodic regimes: one scatters while the other channels.

V. CONCLUSIONS

This work explores the critical role of drift-wave coherence in governing particle transport dynamics in edge plasmas. By truncating the Hasegawa–Mima equation to a three-wave system with dissipative coupling, we identified two distinct transport regimes: hyperballistic motion with $\alpha > 2$ under periodic wave amplitudes, driven by coherent zonal flows that channel particles poloidally, and superdiffusive diffusion under chaotic wave amplitudes, where non-periodic fields disrupt directional coherence. The diffusion coefficient analysis demonstrated that transitions between these regimes are controlled by the behavior of the wave amplitude, governed by the energy exchange coefficient μ_1.

The observed hyperballistic transport, characterized by $\alpha \approx 2.1$, aligns with particles "surfing" coherent potential structures, akin to zonal flows or streamers. In contrast, chaotic wave amplitudes suppress large-scale migration by scattering particles through transient turbulent eddies, reducing α to ≈ 1.4. Particle tracking simulations further revealed that periodic waves enhance radial confinement while enabling rapid poloidal transport, whereas chaotic fluctuations homogenize displacement distributions, reflecting isotropic scattering. These results underscore the dual role of turbulence: while fully chaotic fields degrade confinement, intermediate coherence enables self-organized flows that enhance transport efficiency.

Our findings connect reduced order models and weak turbulent systems, demonstrating that simplified three-wave interactions capture essential features of zonal flow formation and transport bifurcations.

ACKNOWLEDGMENTS

This work has been partially supported by the following Brazilian government agencies: CAPES (Grant Nos. 88887.898818/2023-00 and 88881.143103/2017-01), CNPq (Grant Nos. 140920/2022-6, 304616/2021-4, 403120/2021-7, and 301019/2019-3), and FAPESP (Grant No. 2024/05700-5). The authors are indebted to Professor Edson Denis Leonel for useful discussions and comments.

AUTHOR DECLARATIONS

Conflict of Interest

The authors have no conflicts to disclose.

Author Contributions

Pedro Haerter: Conceptualization (equal); Data curation (equal); Formal analysis (equal); Funding acquisition (equal); Investigation (equal); Methodology (equal); Project administration (equal); Resources (equal); Software (equal); Supervision (equal); Validation (equal); Visualization (equal); Writing – original draft (equal); Writing – review & editing (equal). **Ibere Luiz Caldas:** Conceptualization (equal); Funding acquisition (equal); Methodology (equal); Supervision (equal); Writing – review & editing (equal). **Ricardo Luiz Viana:** Conceptualization (equal); Formal analysis (equal); Funding acquisition (equal); Investigation (equal); Methodology (equal); Project administration (equal); Supervision (equal); Validation (equal); Writing – original draft (equal); Writing – review & editing (equal).

DATA AVAILABILITY

Data sharing is not applicable to this article as no new data were created or analyzed in this study.

REFERENCES

[1]W. Horton and A. Hasegawa, "Quasi-two-dimensional dynamics of plasmas and fluids," Chaos **4**, 227–251 (1994).
[2]P. H. Diamond, S.-I. Itoh, K. Itoh, and T. S. Hahm, "Zonal flows in plasma—a review," Plasma Phys. Controlled Fusion **47**, R35 (2005).
[3]A. Hasegawa and K. Mima, "Pseudo-three-dimensional turbulence in magnetized nonuniform plasma," Phys. Fluids **21**, 87–92 (1978).
[4]A. Hasegawa and K. Mima, "Stationary spectrum of strong turbulence in magnetized nonuniform plasma," Phys. Rev. Lett. **39**, 205–208 (1977).
[5]P. W. Terry, "Suppression of turbulence and transport by sheared flow," Rev. Mod. Phys. **72**, 109–165 (2000).
[6]X. Garbet, P. Mantica, C. Angioni, E. Asp, Y. Baranov, C. Bourdelle, R. Budny, F. Crisanti, G. Cordey, L. Garzotti, N. Kirneva, D. Hogeweij, T. Hoang, F. Imbeaux, E. Joffrin, X. Litaudon, A. Manini, D. C. McDonald, H. Nordman, V. Parail, A. Peeters, F. Ryter, C. Sozzi, M. Valovic, T. Tala, A. Thyagaraja, I. Voitsekhovitch, J. Weiland, H. Weisen, A. Zabolotsky, and T. J. E. Contributors, "Physics of transport in tokamaks," Plasma Phys. Controlled Fusion **46**, B557–B574 (2004).
[7]B. D. Scott, "Energetics of the interaction between electromagnetic ExB turbulence and zonal flows," New J. Phys. **7**, 92 (2005).
[8]A. M. Batista, I. L. Caldas, S. R. Lopes, R. L. Viana, W. Horton, and P. J. Morrison, "Nonlinear three-mode interaction and drift-wave turbulence in a tokamak edge plasma," Phys. Plasmas **13**, 042510 (2006).
[9]W. Horton, "Onset of stochasticity and the diffusion approximation in drift waves," Plasma Phys. Controlled Fusion **27**, 937 (1985).
[10]R. M. Castro, M. V. A. P. Heller, I. L. Caldas, R. P. da Silva, Z. A. Brasilio, and I. C. Nascimento, "Temperature fluctuations and plasma edge turbulence in the Brazilian tokamak TBR," Phys. Plasmas **3**, 971–977 (1996).
[11]E. A. Belli, J. Candy, and R. E. Waltz, "Reversal of simple hydrogenic isotope scaling laws in tokamak edge turbulence," Phys. Rev. Lett. **125**, 015001 (2020).
[12]E. Ott, *Chaos in Dynamical Systems*, 2nd ed. (Cambridge University Press, Cambridge, 2002).

[13]G. I. de Oliveira, L. P. L. de Oliveira, and F. B. Rizzato, "Nonintegrable three mode interaction in the Zakharov equations," Phys. D **104**, 119–126 (1997).
[14]P. W. Terry, "Drift wave turbulence in a low-order k space," Phys. Fluids **26**, 106 (1983).
[15]R. G. Kleva and J. F. Drake, "Stochastic E × B particle transport," Phys. Fluids **27**, 1686–1698 (1984).
[16]G. Z. dos Santos Lima, Z. O. Guimarães-Filho, A. M. Batista, I. L. Caldas, S. R. Lopes, R. L. Viana, I. C. Nascimento, and Y. K. Kuznetsov, "Bicoherence in electrostatic turbulence driven by high magnetohydrodynamic activity in Tokamak Chauffage Alfvén Brésilien," Phys. Plasmas **16**, 042508 (2009).
[17]M. V. A. P. Heller, R. M. Castro, I. L. Caldas, Z. A. Brasílio, R. P. d Silva, and I. C. Nascimento, "Correlation between plasma edge electrostatic and magnetic oscillations in the Brazilian tokamak TBR," J. Phys. Soc. Jpn. **66**, 3453–3460 (1997).
[18]See https://www.boost.org/doc/libs/1_87_0/libs/numeric/odeint/doc/html/index.html for K. Ahnert and M. Mulansky, "Boost numeric Odeint - 1.87.0" (2025).
[19]P. Siegle, I. Goychuk, and P. Hänggi, "Origin of hyperdiffusion in generalized Brownian motion," Phys. Rev. Lett. **105**, 100602 (2010).
[20]D. Gamba, B. Cui, and A. Zaccone, "Hyperballistic transport in dense systems of charged particles under AC electric fields," Phys. Rev. E **110**, 054137 (2024).
[21]M. G. Shats, W. M. Solomon, and H. Xia, "Turbulent transport reduction and randomization of coherent fluctuations by zonal flows in toroidal plasma," Phys. Rev. Lett. **90**, 125002 (2003).
[22]X. Leoncini, O. Agullo, S. Benkadda, and G. M. Zaslavsky, "Anomalous transport in Charney-Hasegawa–Mima flows," Phys. Rev. E **72**, 026218 (2005).